Research in Astron. Astrophys. **2009** Vol. **9** No. **4**, 449–456
http://www.raa-journal.org *http://www.iop.org/journals/raa*

***R**esearch in*
***A**stronomy and*
***A**strophysics*

Non-thermal emission from Vela X and PWN G0.9+0.1 *

Wei-Fan Qiao, Li Zhang and Jun Fang

Department of Physics, Yunnan University, Kunming, 650091, China; *lizhang@ynu.edu.cn*

Received 2008 May 27; accepted 2008 July 2

Abstract We study the multi-waveband non-thermal emission from the pulsar wind nebulae (PWNe) Vela X and G0.9 + 0.1 in the frame of a time-dependent model describing non-thermal radiation from the PWNe. In such a model, the relativistic wind of particles driven by a central pulsar blows into the ambient medium and creates a termination shock that accelerates the particles to very high energy in a PWN. The non-thermal photons in the PWN are produced both by synchrotron radiation and the inverse Compton process, with electrons coming directly from the pulsar magnetosphere and electrons being accelerated at the termination shock. We apply this model to reproduce the observed multi-waveband photon spectra of Vela X and the G0.9+0.1, both of which have been detected emitting very high energy photons. Our results indicate that TeV photons are produced by the inverse Compton scattering of the high-energy electrons in the infrared photon field in both Vela X and PWN G0.9+0.1. The TeV photons from these two PWNe may have leptonic origins.

Key words: ISM: individual objects: Vela X, G0.9 + 0.1 — gamma-rays: theory

1 INTRODUCTION

Seven pulsar wind nebulae (PWNe) have been detected emitting very high energy (VHE) gamma-rays, including the Crab Nebula, MSH15–52, Vela X, HESS J1825–137, PSRJ1420-6049, the Rabbit and G0.9 + 0.1 (e.g. Gallant 2007; Hinton 2007). These observations provide some information for us to study acceleration mechanisms and radiation processes inside PWNe, and show evidence for the acceleration of particles up to very high energies inside some PWNe.

It is generally believed that a pulsar converts its spin-down power into a relativistic wind. This wind interacts with the surrounding supernova ejecta and is reduced to form a termination shock in order to match the boundary condition of non relativistic expansion of the confining supernova remnant, leading to the formation of a PWN. In such a picture, a non-negligible fraction of the energy lost by the pulsar may become detectable in the form of non-thermal radiation emitted by the relativistic particles in the PWN (e.g. Volpi et al. 2008). In order to explain the observed broad band spectrum of nonthermal radiation, typically extending from the radio to the X-ray and even gamma-ray bands, various models have been proposed. These models are divided into two classes: leptonic models and hadronic-leptonic models. In the leptonic models, the non-thermal radiation in a PWN is produced by leptons in the synchrotron and the inverse Compton processes (e.g. de Jager & Harding 1992; Atoyan & Aharonian 1996; Hillas et al. 1998; Aharonian et al. 2004; Zhang et al. 2008). In the hadronic-leptonic models, however, both leptons and hadrons are assumed to contribute to the non-thermal emission from a PWN; in particular, the hadronic contribution may dominate in the VHE energy range (e.g. Bednarek & Bartosik 2003, 2005; Horns et al. 2006). In this paper, we will focus on the leptonic models.

∗ Supported by the National Natural Science Foundation of China.

Recently, Zhang et al. (2008) have studied the non-thermal emission of PWNe from radio to TeV gamma-ray bands based on a simplified time-dependent injection model. In the model, a relativistic wind of particles driven by a central pulsar with a spin-down power goes into the ambient medium and a shock wave is formed to accelerate the particles to very high energies through the Fermi acceleration mechanism in the PWN. The non-thermal photons in the PWN are produced by synchrotron radiation and the inverse Compton process (the synchrotron-self Compton (SSC) process for the Crab Nebula), with electrons coming directly from the pulsar magnetosphere and electrons being accelerated at the termination shock. Zhang et al. applied the model to explain the observed multi-waveband non-thermal radiation of the Crab Nebula, MSH 15–52, and HESS J1825–137. In this paper, we will apply this model to Vela X and G0.9+0.1. For Vela X, Horns et al. (2006) suggested that TeV photons originate from proton–proton interaction. Our result indicates that TeV emission from Vela X can also be explained as the inverse Compton scattering of the relativistic electrons. For G0.9 + 0.1, Venter & de Jager (2006) studied constraints on the parameters of the unseen pulsar in PWN G0.9+0.1 by using observed radio, X-ray and VHE gamma-ray data.

The paper is organized as follows. In Section 2, we briefly review the leptonic model given by Zhang et al. (2008). We apply this model to explain the observed multi-waveband photon spectra of Vela X and G0.9+0.1 in Section 3. Finally, we give our conclusions and discussion in Section 4.

2 THE MODEL

We now briefly describe the time-dependent model for the non-thermal photon emission of a PWN given by Zhang et al. (2008). In this model, the relativistic wind of electrons produced within the light cylinder of the pulsar with a spin-down power $L(t)$ is injected into a PWN, and flows freely out until its pressure is balanced by that of the surrounding medium, where the wind decelerates and a standing termination shock is formed, leading to acceleration of the particles (e.g. Kennel & Coroniti 1984; Aharonian, Atoyan & Kifune 1997). Therefore, the relativistic electrons usually contain two components: one (called the radio electron component) is produced inside the light cylinder of the pulsar, and the other (called the wind electron component) is produced beyond the light cylinder at the shock radius by a Fermi-type process (Achterberg et al. 2001). The injected spectrum of such relativistic electrons can be approximated as a broken power law with indices α_1 and α_2, and breaking energy $E_{\rm b}$ (Venter & de Jager 2006), namely

$$Q(E_e,t)=\begin{cases} Q_0(t)\left(\frac{E}{E_{\rm b}}\right)^{-\alpha_1} & E<E_{\rm b} \\ Q_0(t)\left(\frac{E}{E_{\rm b}}\right)^{-\alpha_2} & E\geq E_{\rm b}\ , \end{cases} \tag{1}$$

where the radio electrons dominate below the $E_{\rm b}$ and the wind electrons dominate above the $E_{\rm b}$. This injected spectrum can be related to the spin-down power $L(t)$ of the pulsar at time t by assuming that part of the spin-down power is converted into particle luminosity, i.e. $\int Q(E,t)EdE=\eta L(t)$, where η is the conversion efficiency.

For a given pulsar, the evolution of spin-down power $L(t)$ is given by

$$L(t)=L_0\left[1+\frac{(n-1)P_0^2L_0t}{4\pi^2I}\right]^{-\frac{n+1}{n-1}}, \tag{2}$$

where L_0 and P_0 represent the spin-down power and pulsar period at pulsar birth respectively, n is the braking index and I is the moment of inertia. A pulsar begins its life with a spin-down luminosity which drives the particle wind into the ambient medium. The maximum energy of the accelerated particles can be limited by the requirement that the electron Larmor radius $r_{\rm L}$ must be less than half the radius of the PWN (Zhang et al. 2008), $r_{\rm L}\leq 0.5r_s$, resulting in

$$E_{\rm max}(t)=\frac{e}{2}\sqrt{\frac{\sigma L_t}{(1+\sigma)c}}\ . \tag{3}$$

The magnetization parameter σ is defined as $\sigma = (B^2/8\pi)(nu\gamma mc^2/2)$, where B is the magnetic field, n is the density, γ is the Lorentz factor of the relativistic electrons and $u = \sqrt{\gamma^2 - 1}$ is the radial 4-speed of the relativistic electron flow at the shock. Sefako & de Jager (2003) considered geometric effects on the compact nebular spectrum and obtained $\eta = \Omega_E/4\pi(1+\sigma)$, where $\Omega_E = 4\pi \sin\theta_E$ is the solid angle accounting for the fact that the synchrotron emission in the compact nebula is not isotropic, but rather confined to a torus with half-opening angle θ_E. Here, we set $\eta \sim 0.1$ as a parameter.

The temporal evolution of the electron energy distribution can be investigated when the injection rate of the relativistic electrons is given. The equation for electrons in energy space can be given by

$$\frac{dn_e(E,t)}{dt} = Q(E,t) - \frac{n_e(E,t)}{\tau_{\rm syn}(t)} - \frac{n_e(E,t)}{\tau_{\rm esc}(t)} \ , \tag{4}$$

where $n_e(E,t)$ is the differential electron density and $\tau_{\rm syn}$ is the lifetime of a relativistic electron with respect to the synchrotron energy loss, which is given by

$$\tau_{\rm syn}(t) \approx 15.75\Big(\frac{B(t)}{4\times10^{-4}\,{\rm G}}\Big)^{-2}\Big(\frac{\gamma}{10^7}\Big)^{-1}{\rm yr} \ , \tag{5}$$

where γ is the Lorentz factor of the injected electrons. $\tau_{\rm esc}(t)$ is the escape timescale,

$$\tau_{\rm esc}(t) \approx 7.1\times10^5\Big(\frac{B(t)}{4\times10^{-4}\,{\rm G}}\Big)\Big(\frac{\gamma}{10^7}\Big)^{-1}\Big(\frac{R_{\rm PWN}}{\rm pc}\Big)^2{\rm yr} \ , \tag{6}$$

where $R_{\rm PWN}$ is the PWN radius. In Equations (5) and (6), the magnetic field inside the PWN needs to be calculated by the value of the field strength and r_s. The magnetic field in the PWN changes with time and can be modeled as (Venter & Jager 2006)

$$B(t) = \frac{B_0}{1+(\frac{t}{\tau_0})^\alpha} \ , \tag{7}$$

where α is the B-field parameter and τ_0 is the characteristic time-scale.

The number of particles contained in the PWN at energy E when $t = T_{\rm age}$ can be given by

$$\frac{dN(E,T_{\rm age})}{dE} = \int_0^{T_{\rm age}} Q(E,t)\exp\Big(-\frac{T_{\rm age}-t}{\tau_{\rm eff}}\Big), \tag{8}$$

where $\tau_{\rm eff}^{-1} = \tau_{\rm syn}^{-1} + \tau_{\rm esc}^{-1}$.

When time-dependent electron and proton intensities are determined, multi-wavelength non-thermal photons can be calculated. The non-thermal component consists of electron synchrotron radiation and inverse Compton scattering of the soft seed photons. Below, we briefly introduce these photon production processes (see Zhang & Fang for details).

For synchrotron radiation, the emissivity is given by

$$Q_{\rm syn}(E_\gamma,t) = \Big(\frac{2\sqrt{3}e^3B}{\hbar E_{\gamma m_e c^3}}\Big)\int_0^{\pi/2} d\theta\sin^2\theta\int_{E_{e,\rm min}}^{E_{e,\rm max}} dE_e J(E_e,t)F\Big(\frac{E_\gamma}{E_c}\Big), \tag{9}$$

where $J_e(E) = J_e(E,T_{\rm age}) = (c\beta/4\pi)dN(E,T_{\rm age})/dE$, θ is the electron pitch angle, $E_c = 4.2\times10^6 hB\gamma_e^2\sin\theta$, B is the local magnetic field strength and

$$F(y) = y\int_y^\infty dz K_{5/3}(z) \ , \tag{10}$$

with $y = E_\gamma/E_c$, where $K_{5/3}$ is a modified Bessel function of order 5/3.

For the Compton process, we use the full Klein–Nishina cross section for relativistic electrons to calculate the emissivity, which is

$$Q_{\mathrm{comp},j}(E_\gamma,t)=4\pi\int_0^\infty d\epsilon n_j(\epsilon,r)\int_{E_{e,\min}}^{E_{e,\max}}dE_eJ_e(E_e,t)F(\epsilon,E_\gamma,E_e)\ \ , \tag{11}$$

where $E_{e,\min}=[E_\gamma+(E_\gamma^2+E_\gamma(m_ec^2)^2/\epsilon)^{1/2}]/2$ is the lowest energy that electrons can scatter a target photon with energy ϵ to energy E_γ, ϵ is the target photon energy and n_j is the number density of soft photon component j. The energy distribution component of CMB, IR and star light can be given by

$$n_j(\epsilon)=\frac{15U_j}{(\pi kT_j)^4}\frac{\epsilon^2}{\exp(\epsilon/kT_i)-1}\,. \tag{12}$$

The energy density of the synchrotron photons is (Atoyan & Aharonian 1996)

$$n_{\mathrm{syn}}(r,\epsilon)=\frac{Q_{\mathrm{syn}}(\epsilon)}{4\pi r_0^2c}U(x)\,, \tag{13}$$

$$U(x)=\frac{3}{2}\int_0^1\frac{y}{x}\ln\frac{x+y}{|x-y|}dy\,, \tag{14}$$

where $x\equiv r/r_0$ and $Q_{\mathrm{syn}}(\epsilon)$ is the synchrotron emissivity. In Equation (13), it is assumed that the synchrotron emission is homogeneous in the nebula with average emission volume $V_0=\frac{3}{2}\pi r_0^2$. Function $F(\epsilon,E_\gamma,E_e)$ is given by

$$F(\epsilon,E_\gamma,E_e)=\frac{3\sigma_T}{4(E_e/mc^2)^2}\frac{1}{\epsilon}\Big[2q\ln q+(1+2q)(1-q)+\frac{(\Gamma q)^2(1-q)}{2(1+\Gamma q)}\Big]\,, \tag{15}$$

where $\Gamma=4\epsilon(E_e/mc^2)/mc^2$, $q=E_1/\Gamma(1-E_1)$, $E_1=E_\gamma/E_2$, $1/4(E_e/mc^2)<q<1$.

3 APPLICATION

3.1 Vela Nebula

The pulsar Vela (PSR B0833–45) is the brightest one at radio bands with a rotational period of 89.3 ms and a period derivative 1.274×10^{-13} s/s, corresponding to a current spin-down luminosity of 7×10^{36} erg s^{-1} (Taylor et al. 1993). With observational data of proper motion and parallax of Vela, the distance to the pulsar can be approximated as 290^{+19}_{-17} pc (Dodson et al. 2003).

Helfand et al. (2001) performed a high-resolution Chandra X-ray observation for the 89 ms pulsar PSR B0833–45. It is also the first observation showing a significant "ghost image", in which appears a residual jet-like feature. The thermal X-ray emission extends to the edge of the Vela SNR and the Chandra X-ray image shows a compact nebula with a jet–counter jet originating from the pulsar and a double bow structure (Helfand et al. 2001). The jet is believed to interact with the supernova remnant. The spectrum with energies from 2 to 10 keV is harder near the pulsar and becomes soft at a distance of $2'-3'$ (Kargaltsev & Pavlov 2003).

In the PWN, the radio, X-ray and VHE gamma-ray emission regions are all markedly offset from the pulsar position. This may be due to the supernova explosion occurring in an inhomogeneous medium, and the resulting asymmetric reverse shock displaces the PWN in the direction away from the higher density medium (Blondin et al. 2001).

At VHE γ-ray energies, Vela has been detected by HESS (Aharonian et al. 2006). The TeV γ-rays come from the inner section of the SNR and the overall energy spectrum can be fitted by a power law with photon index $\Gamma=1.45\pm0.09_{\mathrm{stat}}\pm0.2_{\mathrm{sys}}$ in the 550 GeV and 65 TeV and an exponential cutoff at an energy of $13.8\pm2.3_{\mathrm{stat}}\pm4.1_{\mathrm{sys}}$ TeV.

The initial spin period can be estimated as $P_0 = 0.04632\,\mathrm{s}$ by using the braking index $n = 1.5$. Because $L_t \approx 7.0 \times 10^{36}\,\mathrm{erg\,s^{-1}}$ for $I = 3 \times 10^{45}\mathrm{g\,cm^2}$, we can get L_0 from Equation (1). Based on the Chandra observations, Gaensler et al. (2002) derived $\sigma = 3.5 \times 10^{-2}$ and a nebular magnetic field greater than $5\,\mu$G. The final parameters we choose are shown in Table 1 and the resulting non-thermal spectra with X-ray and VHE γ-ray observations are shown in Figure 1. The observed X-ray emission from the PWN is from the synchrotron radiation whereas the TeV photons are produced mainly via inverse Compton scattering off the soft IR photons.

Table 1 Values of Parameters Used in the Modeling

Model parameter	Symbol	G0.9+0.1	Vela
Breaking index	n	3	1.5
B-field parameter	α	0.5	0.5
Present-day B-field	$B(t)$	25 μG	6.3 μG
Conversion efficiency	η	0.2	0.01
Age	T	6500 yr	11 000 yr
Characteristic time scale	τ_0	500 yr	500 yr
Distance	d	8.5 kpc	0.29 kpc
Magnetization parameter	σ	3.0×10^{-1}	3.5×10^{-2}
Moment of inertia	I	3×10^{45} g cm^2	3×10^{45} g cm^2
Q break energy	E_b	0.8×10^5 MeV	1.0×10^5 MeV
Q index 1	α_1	–1.7	–1.9
Q index 2	α_2	–2.9	–2.1
Initial spin-down power	L_0	3×10^{38} erg s^{-1}	7.5×10^{36} erg s^{-1}
Birth period	P_0	0.043 s	0.04632 s
Average PWN radius	r_PWN	10 pc	10 pc
Average SynE radius	r_0	5 pc	3 pc

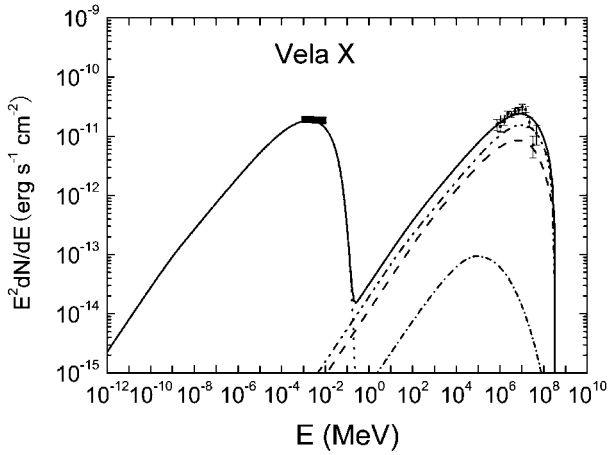

Fig. 1 Comparison of predicted multi-waveband spectrum of Vela X with the observed data. The observed data at X-ray and VHE γ-ray bands are taken from Markwardt & Ögelman (1997) and Aharonian et al. (2006), respectively. The synchrotron emission (dotted line) and the inverse Compton scattering with CMB (dash-dot-dotted line), IR (dashed line), starlight (short dash-dotted line) and the total emission (solid line) calculated with our model are shown.

The observed data of Vela X at X-ray and VHE γ-ray bands are taken from Markwardt & Ögelman (1997) and Aharonian et al. (2006), respectively. The four different seed photons in Vela X are (1) the 2.7 K CMB radiation, with energy density $U_{\rm CMB} = 0.25\,{\rm eV\ cm^{-3}}$; (2) the IR, with energy density $U_{\rm IR} = 0.5\,{\rm eV\ cm^{-3}}$ and temperature 25 K; (3) the starlight, with energy density $U_{\rm star} = 0.5\,{\rm eV\ cm^{-3}}$ and temperature 5000 K; and (4) the synchrotron radiation in the nebula.

3.2 G0.9+0.1 Nebula

G0.9+0.1 is a composite supernova remnant which is located in the Galactic Center, with a distance of 8.5 kpc and an age of 6500 yr (Mezger et al. 1996; Helfand & Becker 1987). A nebula wind has been detected in the center of G0.9+0.1 by radio observations (Helfand & Becker 1987). The steep radio spectrum gives us a chance to further study the central bright PWN. In the X-ray band, the central pulsar wind nebula was first detected with Bepposax (Mereghetti & Sidoli 1998; Sidoli et el. 2000). The X-ray data has a power-law spectrum with a photon index $\Gamma = 2.03$ with energies from 2 to 10 keV. Recently, VHE γ-rays were detected from the G0.9+0.1 Nebula with a stereoscopic system of five image air Cherenkov telescopes that was part of the High Energy Gamma Ray Astronomy (HEGRA) experiment. The spectrum was extended to 200 GeV, and the VHE γ-ray spectrum can be approximately expressed as a power law with photon index $2.4\,\pm 0.11_{\rm stat} \pm 0.20_{\rm sys}$.

Helfand & Becker (1987) used the VLA to observe the bright radio source in G0.9+0.1 near the Galactic Center in 1984. They argued that the SNR G0.9+0.1 consists of a radio polarized core component surrounded by a shell with a steeper radio spectrum (Helfand & Becker 1987). Helfand and Becker constructed a broad band spectrum (radio – X-ray) to compare the X-ray and the infrared emissions (Venter & Jager 2006). The core to shell morphology was detected by VLA observations at 20 and 90 cm and La Rosa et al. (2000) measured spectral indices of $\sim$0.77 for the shell and of $\sim$0.12 for the core in the component SNR G0.9+0.1. The observed data with BeppoSAX gave more stringent upper limits on the pulsation (in the range of periods from 4 ms to $\sim 4\times 10^4$ s). The observation also gave an upper limit on the 2–10 keV X-ray data from the radio shell and marginal evidence of an X-ray plerion (Sidoli et al. 2000). It is uncertain whether there exists a pulsar in the center of G0.9+0.1, but it is clear that the X-ray observation originates from the plerion rather than from the shell (Sidoli et al. 2000). Helfand & Becker (1987) argued that the relativistic particles accelerated in the core, which is a PWN, and produced the non-thermal photons through synchrotron radiation. Hard X-rays were also detected by XMM-Newton (Porquet et al. 2003). The data show X-ray sources with energies ranging from 1.5 to 12 keV and the core of the PWN is surrounded by extended diffuse emission. In this band, the flux is in accord with the upper limit of Sidoli et al. (2000). There are two X-ray sources in the east where the X-ray peak matches the X-ray core and in the west where the radio peak corresponds to an X-ray arc-like feature of PWN G0.9+0.1.

In order to calculate the broadband spectrum of the G0.9+0.1 Nebula, we first need to determine the pulsar parameters. For G0.9+0.1, $n = 1.5$, $P_0 = 0.043$ s, $T \approx 1.1 \times 10^4$ yr and $d = 8.5$ kpc are known; the spin-down $L(t)$ at the present time is estimated as $L(t) = 3 \times 10^{38}\,{\rm erg\ s^{-1}}$. We choose a breaking energy of $E_{\rm b} = 0.8 \times 10^5$ MeV to fit the observational data, in good agreement with the parameter of Venter & de Jager (2006). Finally, we need the parameters of the PWN. The magnetic field is chosen to be $25 \times 10^{-6}\,\mu$G to be consistent with the observations, which is greater than that used by Venter & de Jager (2006) by a factor of about 4.

Application of the simplified temporal model to the G0.9+0.1 yields the parameters shown in Table 1. The resulting broadband spectrum is shown in Figure 2 along with the radio (Helfand & Becker 1987), X-ray (Porquet et al. 2003) and VHE data (Aharonian et al. 2005). It is obvious that synchrotron emission dominates the spectrum from radio to 10 MeV; the higher energy photons are produced by inverse Compton scattering with soft seed photons. The four different seed photons in the G0.9+0.1 are as follows: (1) the 2.7 K CMB radiation, with energy density $U_{\rm CMB} = 0.25\,{\rm eV\ cm^{-3}}$; (2) the IR radiation, with energy density $U_{\rm IR} = 0.5\,{\rm eV\ cm^{-3}}$ and temperature 25 K; (3) the starlight, with energy density $U_{\rm star} = 0.15\,{\rm eV\ cm^{-3}}$ and temperature 5000 K; and (4) the synchrotron radiation in the nebula.

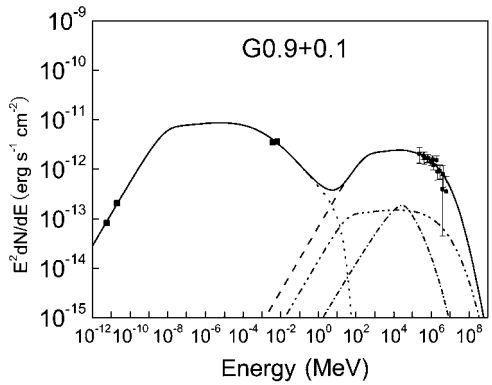

Fig. 2 Comparison of predicted multi-waveband spectrum of PWN G0.9+0.1 with the observed data. The observed radio, X-ray and VHE γ-ray data are taken from Helfand & Becker (1987), Porquet et al. (2003) and Aharonian et al. (2005), respectively. The synchrotron emission (dotted line), inverse Compton scattering with CMB (dash-dot-dotted line), IR (dashed line), starlight (short dash-dotted line), synchrotron photons (dash-dotted line) and the total emission (solid line) calculated with our model are shown.

4 CONCLUSIONS AND DISCUSSION

In this paper, based on a temporal non-thermal model of PWNe given by Zhang et al. (2008), we have studied the multi-band non-thermal spectra for Vela X and G0.9+0.1, respectively. With appropriate parameters (see Table 1), our predicted multi-band spectra for these two PWNe are consistent with the observed data (see Figs. 1 and 2). Our results indicate that the non-thermal emission range from the radio to the X-ray band is from the synchrotron radiation of non-thermal electrons, whereas the VHE γ-rays are usually produced through inverse Compton scattering on the soft seed photons for a PWN, namely, the non-thermal emission from radio to VHE gamma-ray bands for these two PWNe may have a leptonic origin.

For Vela X, Horns et al. (2006) (see also Horns et al. 2007) proposed a nucleonic gamma-ray production model, in which ions in the relativistic pulsar wind drive particle acceleration and are expected to produce gamma-ray emission via inelastic scattering with the ambient medium. In such a model, the synchrotron and inverse Compton emission from primary and secondary electrons are included and the model results are compared with observational data. Horns et al. (2006) concluded that the observed gamma-ray emission can be produced by a pulsar wind which carries a large fraction of the spin-down luminosity in the form of relativistic nuclei; their detailed calculation shows that the required energy in the nuclei is about 10^{49} erg for protons and 10^{48} erg for iron nuclei released in the pulsar wind. However, de Jager & Djannati-Ataï (2008) pointed out that the total energy budget in Vela X implied by the HESS detection should be greater than that given by Horns et al. (2006), and the total integrated kinetic energy provided by the pulsar since birth is $\sim 1.2 \times 10^{49}$ erg, indicating a conversion efficiency of $> 100\%$ of spin-down power to ions in Vela X, which is physically impossible. Therefore, de Jager & Djannati-Ataï (2008) concluded that VHE emission in Vela X is more likely to be of leptonic than hadronic origin, which is consistent with our prediction. For PWN G0.9+0.1, Venter & de Jager (2006) only gave the best fits at radio, X-ray and VHE gamma-ray bands respectively, and did not obtain the best fit of the total spectrum from radio to VHE gamma-ray bands. In our calculation, in order to reproduce the observed multi-waveband spectrum well, some parameters such as $B(T)$, α_1, α_2, σ and so on used in this paper (see Table 1) are different from those used by Venter & de Jager (2006). Since there are some uncertainties in the model parameters, we expect that a future study can give better constraints on the model parameters we used here.

Acknowledgements This work is partially supported by grants from the National Natural Science Foundation of China (NSFC, Nos. 10778702 and 10778726).

References

Achterberg, A., et al. 2001, MNRAS, 328, 393
Atoyan, A. M., & Aharonian, F. A. 1996, MNRAS, 278, 525
Aharonian, F. A., Atoyan, A. M., & Kifune, T. 1997, MNRAS, 291, 162
Aharonian, F., et al. 2004, ApJ, 614, 897
Aharonian, F., et al. 2005, A&A, 432, L25
Aharonian, F., et al. 2006, A&A, 448, 43
Bednarek, W., & Bartosik, M. 2003, A&A, 405, 689
Bednarek, W., & Bartosik, M. 2005, JPh G, 31, 1465
Blondin, J. M., Chevalier, R. A., & Frierson, D. M. 2001, ApJ, 563, 806
de Jager, O. C., & Harding, A. K. 1992, ApJ, 396, 161
de Jager, O. C., & Djannati-Ataï, A. 2008, in Springer Lecture Notes on Neutron Stars and Pulsars: 40 Years after Their Discovery, eds. W. Becker, arXiV:0803.0116
Dodson, R., Legge, D., Reynolds, J. E., & McCulloch, P. M. 2003, ApJ, 596, 1137
Gaensler, B. M., et al. 2002, ApJ, 569, 878
Gallant, Y. A. 2007, Ap&SS, 309, 197
Helfand, D. J., & Becker, R. H. 1987, ApJ, 314, 203
Helfand, D. J., Gotthelf, E. V., & Halpern, J. P. 2001, ApJ, 556, 380
Hillas, A. M., et al. 1998, ApJ, 503. 744
Hinton, J. 2007, Rapporteur talk at the 30th International Cosmic Ray Conference, Merida, Mexico, arXiV: 0712.3352
Horns, D., et al. 2006, A&A, 451, 51
Horns, D., et al. 2007, Ap&SS, 309, 189
Kargaltsev, O. Y., & Pavlov, G. 2003, in Young Neutron Stars and Their Environment, IAU Symp.218, eds. F. Camilo, & B. M. Gaensler, 195
Kennel, C. F., & Coroniti, F. V. 1984, ApJ, 283, 694
La Rosa, G., Gianotti, F., Fazio, G., Segreto, A., Stephen, J., & Trifoglio, M. 2000, AIPC, 510, 693
Markwardt, C. B., & Ögelman, H. 1997, ApJ, 480, L13
Mereghetti, S., & Sidoli, L. 1998, ApJ, 331, L77
Mezger, P. G., Duchl, W. J., & Zylka, R. 1996 A&ARv., 7, 289
Porquet, D., Decourchelle, A., & Waiwick, R. S. 2003, A&A, 401, 197
Sefako, R. R., & de Jager, O. C. 2003, ApJ, 593,1013
Sidoli, L., Mereghetti, S., Israel, G. L., & Bocchino, F. 2000, A&A, 361, 719
Taylor, J. H., Manchester, R. N., & Lyne, A. G. 1993, ApJS, 88, 529
Volpi, D., Del Zanna, L., Amato, E., & Bucciantini, N. 2008, A&A, arXiv: 0804.1323
Venter, C. & De Jager, O. C. 2006, Proceedings of the 363,WE- heraeus, Seminar on: Neutron Stars and Pulsars, eds. W. Becker, H. H. Huang, MPE Report 291, 40
Zhang, L., & Fang, J. 2007, ApJ, 666, 247
Zhang, L., Chen, S. B., & Fang, J. 2008, ApJ, 676, 1210